Photocatalytic reductive and oxidative ability study of pristine ZnO and CeO2-ZnO heterojunction impregnated with Cu2O

(Article begins on next page)

26 April 2024

Photocatalytic Reductive and Oxidative ability study of pristine ZnO and CeO₂-ZnO heterojunction impregnated with Cu₂O

Erik Cerrato, Paola Calza and Maria Cristina Paganini*[a]

[a] *Dipartimento di Chimica and NIS, University of Turin, Via P. Giuria 7, Torino, Italy*

Abstract

In the present work the Cu_2O-ZnO heterosystem and the novel Cu_2O-CeO_2-ZnO triphasic heterojunction were synthesized impregnating the ZnO and the CeO_2-ZnO system surfaces with 0.5% in weight of Cu_2O, respectively. While X-ray powder diffraction (XRPD) evidenced any alteration in the matrix phases, the UV-vis and electron paramagnetic resonance (EPR) spectroscopy highlighted a drastic change in the optical and electronic behaviour respect to the non-impregnated samples. Deeply investigations allowed us identifying the photo-stability of the surface decorative Cu_2O phase and the presence of additional copper species, namely Cu^{2+} and Cu(0), coming as "waste" from the employed impregnation route. The presented outcomes brought us to suggest a beneficial impact of these species promoting the overall photocatalytic process. Finally, both the oxidative and reductive photocatalytic activity of the produced materials has been evaluated by means the H_2 generation from the water photosplitting process and through the photodegradation of the tolytriazol molecule, respectively, where the novel Cu_2O-CeO_2-ZnO heterojunction exhibited the best performance upon UV-vis and purely visible irradiation.

1. Introduction

Beyond the widely spread applications in transistor, sensor, catalysis, photovoltaic, spintronic and optoelectronic technologies, semiconducting materials have shown promising performances in the overall photocatalytic field [1-3]. The increasing attraction in semiconductor-based photocatalysis has to be deferred since the pioneering study reported by Fujishima and Honda in 1972, in which they displayed the electrochemical photolysis of water using a rutile-TiO_2 anode [4]. This experiment paved the way to explore the semiconductors capability in each branch of the photocatalytic process.

The large accomplishment of semiconducting materials in the photocatalytic field is attributable to their intrinsic nature showing an energy gap between the valence band – VB – full of bounded (valence) electrons, and the conduction band – CB, generally empty of free electrons. When a suitable amount of electromagnetic energy impinges the semiconductor, part of the electrons residing in the VB band can be photo-excited in the CB, where they are free to react with the surrounding environment once reached the surface. On the other hand, the excitation of electrons from the VB leads to the photo-generation of holes in the VB, where they can freely move. Accordingly, the whole photocatalytic process could be ideally divided in two sub-reactions: the reduction carried out by the photo-excited electrons in the CB and the oxidation entailed by the photo-induced holes in the VB [3]. Among all the photocatalytic reactions that had been reported, the photo-reduction of H_2O molecule to H_2, the photo-conversion of CO_2 in useful chemical compounds and the photo-degradation of classical and emerging harmful pollutants are assuming paramount importance in the recent past [5]. Indeed, the growing interest in the photocatalytic field can be easily understood thinking the electromagnetic radiation coming from the sun as an infinite and "clean" source of energy to photo-activate semiconducting materials [6, 7]. Moreover, the sun electromagnetic energy can be stored in the H-H chemical bond through the water photosplitting process; in turn, H_2 represents one of the cleanest fuel that the humanity can assume, generating water vapor as waste product. Concerning the oxidation taking place by holes in the VB, they can covert a water molecule into $OH^\bullet$ radical, the most efficient and no-selective oxidant species able to mineralize hazardous organic molecules in wastewater [8, 9].

Despite the beneficial environmental impact that photocatalytic technologies could actually bring to cope the water and air pollutions challenges as well as the greenhouse effect, its application in large-scale facilities is still constrained. The main reason affecting the spread of the photocatalytic technology resides in the band

gap values of the most stable ad studied transition metal oxide semiconductors, as TiO_2 and ZnO. Indeed, the band gap of such materials in nanopowder size is around 3.3 eV, meaning that just UV photons can allow electrons promotion in the CB and the following induction of holes generation in the VB. As a matter of fact, the UV component of the solar radiation at the earth surface counts around 3% - 5%, not enough to exhaustively photo-activate these materials. Oppositely, the visible component is around the 43%, definitely much more than the UV one [10]. For this reason, a fervent effort has been made to design increasingly improved solar-light responsive semiconductor materials.

Historically, among the most studied photocatalysts based on transition metal oxide semiconductors the ZnO wurtzite phase occupies a prominent position (behind only to TiO_2) thanks to its good chemical stability, a high binding energy of 60 meV, the easy accessibility to different morphology through various low cost synthetic routes, a direct band gap, an adequate oxidative potential for the photoinduced holes in the valence band and non-toxicity [11-13]. As mentioned, zinc oxide exhibits not negligible drawbacks to carry out photocatalytic reactions, among which the band gap width and the reductive potential of the photoexcited electrons in the CB are the most hindering [14]. Doping procedure and the formation of heterojunction with others photoactive materials have been mainly adopted and developed to overcome the shortcomings [15-17]. The first approach provides the introduction of shallow and deep defect levels inside ZnO band gap in such a way that longer wavelengths can be absorbed. The deliberate insertion of a small amount (between 0.5 % and 5%) of metal (Cu, Ag, Mn, Co, Fe and Al) [18-24] and non-metal (C, N and S) elements [25-27] into ZnO lattice has effectively expanded the response of the material towards visible light. However, the generated defect levels often act as recombination centers, reducing the photocatalytic activity. On the other hand, the constitution of intimately photoactive interfaces offers the unique opportunity to couple the employment of visible light with the excitation of photo-induced electrons at much more negative potential. In particular, depending on the nature of the interaction established at the material interfaces the electrons can acquire more negative potential, suitable to reduce water molecules to H_2. The described charge carriers transport at the interface of a heterojunction system has been recently theorized and experimentally verified for ZnO-C_3N_4 [28, 29]. Still, the CeO_2-ZnO photoactive interface shown interesting activities in the photodegradation of pollutants upon visible irradiation. In previous studies, some of us identified the working mechanism at the materials interface, defining an electron transport from ZnO CB to the empty, localized, *4f* orbitals of Ce^{4+} [30, 31]. In this way, the presence of 1% of CeO_2 was enough to increase the lifetime of photo-excited electrons reducing the recombination rate spatially separating the photo-induced charge carriers. Again, although the CeO_2-ZnO heterostructured system promising performances, one of the main limitation is the low negative potential of electrons in ZnO CB. Thus, with the aim to develop a versatile photocatalyst that could entail both photo-induced oxidative and reductive redox reactions the complex triphasic heterojunction Cu_2O-CeO_2-ZnO has been rationalized and produced, depositing 0.5% of Cu_2O at the surface through a facile impregnation process. Cu_2O is a p-type semiconductor exhibiting a narrow bang gap between $2.1 - 2.6$ eV [32, 33]: beyond the absorption edge in the visible range of the solar spectral region, Cu_2O shows an optimal electrons potential in the CB to fulfill the water photosplitting reductive process [34]. Cu_2O-ZnO and, in particular, Cu-doped ZnO hybrid systems have attracted great attention mainly for the production of sensors and photoelectrochemical cells, while the potential as visible light driven photocatalyst is far less explored, especially for H_2 production from the water photosplitting reaction [35-38].

In this work both the oxidative and reductive photo-induced abilities of Cu_2O-ZnO and Cu_2O-CeO_2-ZnO were deeply investigated. In particular, the prepared materials were tested in the H_2 generation from the water photosplitting reaction path and for the photodegradation of tolyltriazole, upon Uv-vis and visible irradiation. The employment of Electron Paramagnetic Resonance (EPR) spectroscopy coupled with *in-situ* visible irradiation has been revealed essential to shade the light regarding the charge carriers mobility at the difference interfaces and to determine the stability of the synthesized compounds. At the best of our knowledge this study represents the first attempt concerning the production of the triphasic Cu_2O-CeO_2-ZnO heterojunction for photocatalytic applications.

2. Materials and Methods

2.1 Samples preparation

The precursors employed for the preparation of the investigated samples were purchased by Sigma Aldrich, and used without any further purification treatment.

ZnO and CeO$_2$-ZnO synthesis

Bare ZnO and ZnO prepared in presence of 1% molar of cerium (labelled CZ1) were synthesized by means a simple, low cost and environmental-friendly precipitation method. The preparation of the pristine sample provides the dissolution of 2.2 g of Zn(CH$_3$COO)$_2$*2H$_2$O in 160 mL of deionized water and 80 mL of CH$_3$CH$_2$OH; after 1h of stirring at room temperature, 120 mL of NaOH aqueous solution were added. The obtained nanoparticles colloidal solution was laid up for two days: following, the precipitate has been recovered *via* filtration and washed three times with deionized water and CH$_3$CH$_2$OH, respectively. The final product was obtained after calcination at 573 K in air for 30h with a slope of 5°C/min and naturally cooled at room temperature.

The mixed system CeO$_2$-ZnO (CZ1), containing 1% molar of cerium atoms, was made adding the corresponding stoichiometric amount of CeCl$_3$*7H$_2$O to the starting mixture.

Surface impregnation of ZnO and CZ1 with Cu$_2$O

The surface impregnation of the ZnO and CZ1 materials with 0.5% in weight of Cu(I) oxide was realized through the so called Benedict reaction.[33] 0.057 g of glucose and 15 mL of NaOH 2.36*10^{-3} M were added at 10 mL of Cu(NO$_3$)$_2$*3H$_2$O 7.9 *10^{-3} M (0.5% in weight on the basis of the oxide photocatalyst) water solution. The originally blue solution was maintained in stirring for 50 min at 343 K, at the end of which results in an orange suspension, as evidence of the cuprous oxide precipitation. In the proposed Benedict reaction, the glucose reduces the Cu^{2+} ions in solution to Cu$^+$, allowing the formation of Cu$_2$O. The impregnation was provided dispersing 1 g of the photocatalyst (ZnO or CZ1) in 20 mL of deionized water and sonicated at 333 K for 10 min. Following, the oxide containing suspension was spilled in the orange colloidal solution containing Cu$_2$O nanoparticle and left in stirring for 10 min at 333 K. Finally, the Cu$_2$O-ZnO (labelled CuZnO) and the Cu$_2$O-CeO$_2$-ZnO (labelled CuCZ1) impregnated materials were recovered by filtration and washed three times with water and CH$_3$CH$_2$OH and dried at 343 K in air.

2.2 Characterization methods

The crystal phase of the synthesized materials before and after the surface impregnation was monitored with X-ray Powder Diffraction (XRPD). The diffraction patterns were recorded with a PANalytical PW3040/60 X'Pert PRO MPD diffractometer using a copper Kα radiation source (0.154056 nm). The intensities were obtained in the 2θ range between 20° and 80°. X'Pert High-Source software was used for data handling and phases identification.

The optical properties were investigated by means UV-Vis absorption spectroscopy, registered with a Varian Cary 5 spectrometer, coupled with an integration sphere for diffuse reflectance (DR) acquisition; the row data were analyzed with a Carywin UV/scan software. A sample of PTFE with 100% reflectance was employed as reference. Spectra were registered in the 200-800 nm range at a scan rate of 240 nm/min with a step size of 1 nm. The measured intensities were converted with the Kubelka-Munk function. The energy gap has been evaluated using the Tauc plot method [39].

The Electronic Paramagnetic Resonance (EPR) spectroscopic measures were conducted with a CW-EPR EMX-Bruker spectrometer operating at X-band (9.5 GHz), equipped with a cylindrical cavity operating at 100 KHz field modulation and interfaced with a computer with WINEPR Acquisition program. The spectra have

been recorded in a bath of liquid nitrogen (77 K). The photo-activity of the synthesized material has been investigated coupled EPR spectroscopy with *in-situ* irradiation, using a 1000 W xenon lamp (Oriel Instruments) equipped with an IR water filter, to whom a band pass filter (Newport-20CGA) at $\lambda \geq 420$ nm (visible light) have been applied.

2.2 Photocatalytic H_2 evolution

The hydrogen evolution test, *via* water photo-splitting reaction, were performed using a 100 mL quartz flask reactor, isolated from external environment. 1 g of photocatalyst powder was suspended in 20 mL of a 10% v/v ethanol aqueous solution and sonicated for 10 min. The irradiation was performed with a 500 W Xe lamp with an irradiance of 80 W/m^2 (measured without filters). A magnetic stirrer was placed at the bottom of the reactor to keep the particles in suspension during the experiment. Prior to illumination, N_2 was purged into the reactor for 15 min to remove atmospheric oxygen. The photocatalytic activity of the ZnO and CZ1 materials previous and after the impregnation of Cu_2O was then monitored by illuminating the suspension for 2h.

To evaluate hydrogen generation a Micro Gas Chromatograph GC490 equipped with a MS5A column using Ar as carrier gas has been employed. A sketch of the designed reactor is reported in the *Supporting material* (S1).

The standard used for the quantification of produced H_2 was purchased by Savio and was of 50 ppm H_2/O_2 in Ar.

2.3 Photocatalytic tests on pollutant abatement

The irradiation experiments were carried out in closed Pyrex cells (40 mm id x 25mm) on 5 mL of suspension in Milli-Q water containing 1 g/L of catalyst and 20 mg/L of the organic compound kept under continuous stirring. The samples were irradiated using a Philips TLK 05 Blacklight lamp (40 W) with a maximum emission of 365 nm. The suspensions were then filtered with Millipore 0.45 µM Millex LCR hydrophilic PTFE filters and analyzed *via* HPLC-UV.

The analyses for tolyltriazole were carried out with a Merck-Hitachi HPLC system equipped with a L-6200A Intelligent Pump, a L-4200 UV-VIS Detector and a six-way Rheodyne valve injection system. Isocratic elution was performed with a mixture of phosphoric acid solution at pH 2.8 and acetonitrile at a flow rate of 1 ml/min. Condition are as follows: 80/20 v/v with retention times of 6.34 min, detection wavelength was 263 nm.

3. Results

3.1 Structural and morphological analysis

Figure 1 reports the XRPD acquisitions of the synthesized samples. All the diffractograms share the recognizable fingerprints of the wurtzite hexagonal phase,[11] characterized by a sharp profile indicating the good crystallinity of the final materials. In the case of CeO_2-ZnO mixed systems (CZ1 and CuCZ1), an additional weak and broad reflection at $2\theta = 28.6°$ appears, as highlighted in the zoom boxes, due to the reflection of the (111) crystallographic planes characterizing the cubic fluorite-like CeO_2 structure: the very low intensity of the reflection and the broad character suggest the presence of small dimension particles, in the range between 5 and 10 nm, as described in our previous works [40, 41].
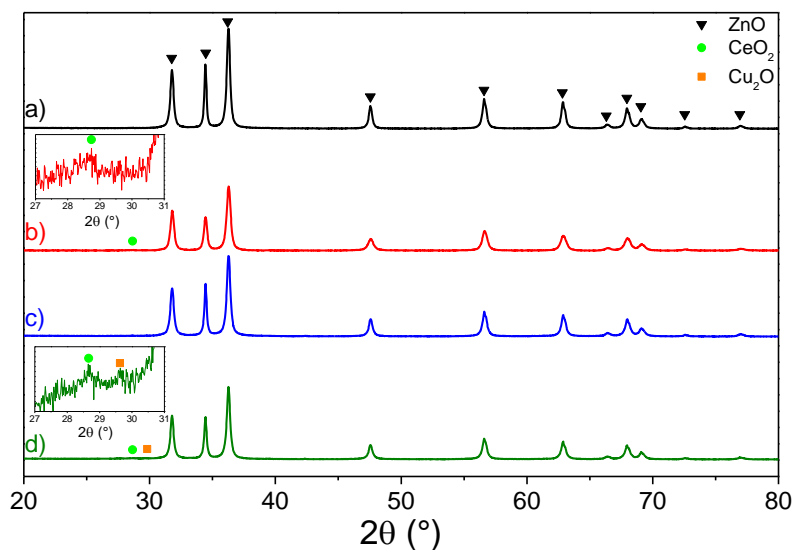
Figure 1. X-ray powder diffraction (XRPD) of: a) pristine ZnO, b) CZ1, c) CuZnO and d) CuCZ1.

A more detailed analysis of the CuZnO and CuCZ1 XRPD patterns allowed us identifying a further extremely tiny reflection at $2\theta = 29.5°$ attesting the presence of Cu_2O phase: it corresponds to the (111) crystallographic planes reflection of the cubic structure of Cu_2O [42]. It is worth mentioning that the most intense reflection of Cu_2O should be visible around $2\theta = 35°$; however, in this case, the low amount of Cu_2O impregnated at the surface (0.5%) does not allow observing this reflection since in that region of the diffractogram the more intense triptych of the wurtzite ZnO structure dominates. Similar to the case of CeO_2, the width of the XRD reflection indicates that the crystal size of Cu_2O nanoparticles should be very small, as it will be discussed in the following by optical and EPR analysis. Still, the reflections of ZnO phase are sharp, staying for a greater crystallinity and larger crystal size respect the other two phases CeO_2 and Cu_2O in the case of CZ1, CuZnO and CuCZ1. Ultimately, no other reflections assignable to additional phases coming from the precursors have been registered, testifying the high purity of the synthesized material.

3.2 Optical analysis

The optical response coming from UV-vis spectroscopy reported in Figure 2 has been crucial to confirmed the presence of the CeO_2 and Cu_2O in the samples CZ1, CuZnO and CuCZ1, supporting XRPD analysis. It is worth to mention that, while the pristine ZnO sample appears of white color (as expected by the band gap width), the addition of 1 molar percentage of cerium as in CZ1 causes a slightly pale yellow color. Still, concerning the impregnated materials they exhibit an antique-pink coloration, due to the presence of Cu_2O at the surface.
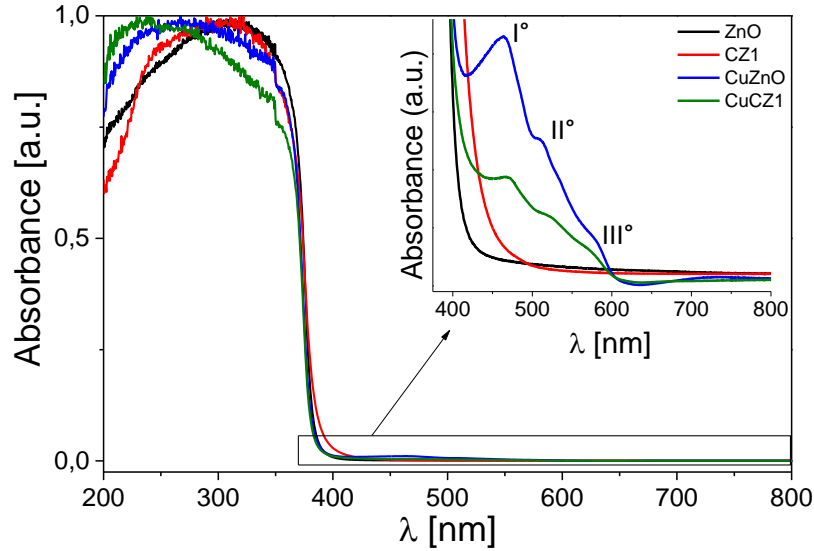
Figure 2. UV- vis analysis *(Absorbance*
Kubelka-Munk *transformed*
diffuse reflectance spectra) of: ZnO (black line), CZ1 (red line), CuZnO (blue line), CuCZ1 (green line).

The normalize absorbance Kubelka-Munk transformed diffuse reflectance spectrum of ZnO reveals the expected absorption at wavelength lower than 400 nm, in the UV range of the electromagnetic spectrum. As widely reported in literature [15, 43-46], the light absorption is due to the excitation of the electrons from the valence band – VB, made up by full *2p* orbitals of O^{2-}, to the conduction band – CB, composed by the empty *4s* states of Zn^{2+}, and characterized by an evaluated direct band gap value of 3.3 eV. Considering the interfaced material CZ1, the presence of CeO_2 does not affect the band gap value; rather it introduces an additional absorption shoulder in the region 400-460 nm. Accordingly, CeO_2 is well known having insulator character with a band gap of 6 eV (for sake of clarity the energy different from the VB to the CB); however, the optical transition (any photon absorption promoting an electron from/to a localized levels inside the material band gap) occurs in the visible region, from the VB, formed by *2p* O^{2-} orbitals, to the intragap states made up by the empty localized *4f* levels of Ce^{4+}, above 2.9 eV in energy from the VB. [40, 47]

The zoom in Figure 2 attests that the impregnation of copper(I) oxide greatly affected the optical absorption feature of the ZnO and CZ1 materials, adding three different contributions (I°, II° and III°) respect to the not impregnated samples. The first one (I° in the magnitude) has been suggested deriving from the interface charge transfer (IFCT) mechanism that may occur from ZnO VB to the present Cu species. The involved electron transfer, promoted by visible frequency, might partially reduce Cu_2O to metallic copper (Cu^0), similarly to what observed for TiO_2 impregnated with Cu_2O and FeO_x. [48, 49] In support of this hypothesis, the broad and low intensity contribution identified as (III°) in the enlargement of Fig. 2 is ascribable to the surface plasmonic resonance (SPR) effect of metallic Cu(0). [50, 51] Finally, the spectral feature labelled as (II°) at almost 520 nm is undoubtedly attributed to the – VB-➔ -CB- electronic transition in Cu_2O. [32]

Definitely, UV-vis spectroscopy has determined that the Cu_2O impregnation dramatically affects the optical properties of the in-object specimens, inducing a higher absorption in the visible region of the electromagnetic spectrum. It is worth mentioning that EPR spectroscopy will help elucidating the presence of different species at the oxides interfaces and their interaction with visible light irradiation, as reported in the next section.

3.3 EPR characterization of the impregnated materials

Electron Paramagnetic resonance spectroscopy evidences the presence of Cu^{2+} species for the impregnated samples CuZnO and CuCZ1 measured at 77 K in vacuum conditions, as reported by the spectra in Fig. 3. Cu^{2+} ion ($3d^9$), differently from Cu^+ and Cu^0 species is paramagnetic, hosting one unpaired electron

6

in the d-orbital with highest energy. The overall signal exhibits an axial g tensor splitted in four hyperfine lines: indeed, the Cu naturally abundant isotopes are characterized by a nuclear spin (**I**) of 3/2. Thus, the expected line multiplicity given by the EPR selection rule is 2**I** + 1 = 4. The intensity of the signal in the two samples is almost the same indicating the reproducibility of the impregnation procedure.

In addition to the fingerprint of the Cu^{2+} species, both the impregnated samples exhibit a further isotropic signal at g = 1.96, arising from the ZnO matrix. In this regard, previous studies in our research laboratories regarding the photoactivity upon visible irradiation of the CeO_2-ZnO heterojunction has highlighted the presence of this signal (see S2).[31, 40] In detail, its origin is to be charged to intrinsic or extrinsic defects hosting an unpaired electron, energetically below just a few meV from the CB edge (then acting as shallow donors) and whose nature is still a question of debate. It has been mainly assigned to intrinsic zinc interstitial defects or hydrogen impurities.[52-55] However, whatever the nature of the defect, the unpaired electrons generating the signal at g = 1.96 can be modeled as in effective-mass-hydrogenetic-like state.[56]

As introduced, the well-known hyperfine structure of Cu^{2+} species appears in the impregnated samples: thinking that in Cu_2O, the copper oxidation state is *1+*, we have to admit that a fraction of the copper supplied during the Benedict reaction has not been reduced efficiently, generating the species at higher oxidation number. However, some important information about the Cu^{2+} species can be derived from the shape and the values of the hyperfine tensor **A**. Indeed, having in mind the Spin Hamiltonian for such a paramagnetic species, reported in equation 1, the interpretation of the hyperfine tensor **A** value can lead to important structural indications.

$$\hat{H} = \beta_e B g \,\hat{S} + \hat{S}^T A \,\hat{I} \qquad (1)$$

where β_e is the Bohr magneton (9.274 10^{-24} J T^{-1}), B is the applied magnetic field in the resonance condition, S is the spin intrinsic magnetic moment with a value of 1/2 for the Cu^{2+} ion, I is the nuclear magnetic moment equal to 3/2 for ^{63}Cu and ^{65}Cu nuclei (natural abundances are 69.17% and 30.83%, respectively), g is the Landè factor and A the hyperfine tensor.

Specifically, the fact that both the perpendicular and the parallel component of the axial **g** and **A** tensors are resolved means Cu^{2+} species are not interacting among them and can be classified as isolated ions, with the corresponding values at $g_{//}$ = 2.355, $g_{\perp}$ = 2.044 and $A_{//}$ =15 mT, $A_{\perp}$ = 3.1 mT, respectively. The situation would be different for clusters of Cu^{2+} ions mutually interacting, in which the dipolar interaction would increase the broadening of the EPR line (dipolar-broadening effect), losing in the resolution of the hyperfine interaction tensor A.[57] Still, we can deduce that Cu^{2+} species coming as "waste" from the impregnation procedure of Cu_2O on the photocatalyst surfaces are not embedded in both the ZnO and CeO_2 lattices since in the given situation the values for the **A** tensors have been found to be decisively smaller than in the in-object study.[58, 59]
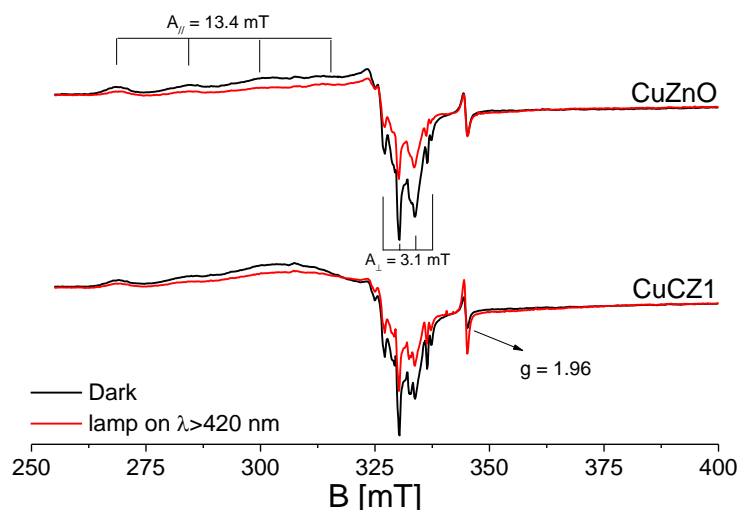
Figure 3. EPR spectra recorded at 77K of CuZnO and CuCZ1 before (black lines) and during irradiation using band pass filter at λ ≥ 420 nm (red line).

It has been worth to investigate the behaviour of the impregnated materials upon visible irradiation (λ ≥ 420 nm), still focusing the attention on the Cu^{2+} signal. It emerges that upon purely visible irradiation, a depletion of the related Cu^{2+} signal occurs: this behaviour can be explained as a partial reduction of the Cu^{2+} species anchored at the surface most likely due to an electron transfer process involving the oxide matrix into the diamagnetic forms Cu^+ or Cu^0. This empirical outcome allows us deducing two significant consequences. The first concerns the stability upon irradiation of the deposited Cu_2O: indeed, it is well known that one of the main material drawback is the photo-stability during light absorption. However, if the impregnated Cu_2O phase was photo-corroded the EPR signal due to Cu^{2+} should have increased instead of decreased; thus, a first interpretation of the reduction of the Cu^{2+} intensity upon irradiation should be read as a stability of the lodged surface material. The second implication regards the fact that Cu^{2+} species are reduced by necessity, since copper cannot have an oxidation number higher than *2+*: then it emerges the Cu^{2+} coming as "waste" from the impregnation procedure at the surface is passing into a more reduced species that can be Cu^+ or metallic copper (both diamagnetic, thus EPR inactive).

3.4 Photocatalytic H_2 evolution

The synthesized materials ZnO, CZ1, CuZnO and CuCZ1 were tested in the redox reduction process for the H_2 production from the water photo-splitting reaction with particular emphasis on the evaluation of the role of the Cu_2O surface impregnation. The irradiation was performed upon UV-vis light and purely visible light again setting the lamp with a band pass filter at λ ≥ 420 nm.

It is worth highlighting at this point of the discussion that the entire water photo-splitting process (eq. 2) is the sum of two half redox reactions: the *hydrogen evolution reaction* (HER) and *oxygen evolution reaction* (OER). In the HER the electron redox ability (depending on the CB potential of the material) is exploited to reduce protons in hydrogen molecules (eq.3). On the other hand, the hole redox propensity (depending on the VB potential) is utilized to oxidize oxygen anions (eq.4). The overall process can be written as hereafter, considering that the highest level of the VB must be more positive than the water oxidation level, equal to 1.23 V in the *Normal Hydrogen Electrode* (NHE) energy scale and the conduction band edge must be more negative than the hydrogen evolution potential (0 V in NHE).

$$H_2O \rightarrow H_2 + \tfrac{1}{2}O_2 \qquad\qquad (2)$$

$$2H^+ + 2e^- \rightarrow H_2 \qquad\qquad E^0_{reduction} = 0.00 \text{ V} \qquad (3)$$

$$H_2O + 2h^+ \rightarrow 2H^+ + 1/2O_2 \qquad\qquad E^0_{oxidation} = +1.23 \text{ V} \qquad (4)$$

In our experimental set up, the μ-GC was connected with a home-made reactor (see S1) to monitor the H_2 produced only, according with the half-reaction involved in the all water photo-splitting process (HER, eq. 3).

In Fig. 4 the hydrogen production after 2h of the corresponding irradiation are reported, evaluated by means of a standard as described in the *Materials and Methods* section. It turns out that after 2h of irradiation the surface modified materials are, in general, more active in the H_2 production respect the unmodified ZnO and CZ1, both under UV-vis ad purely visible irradiation.
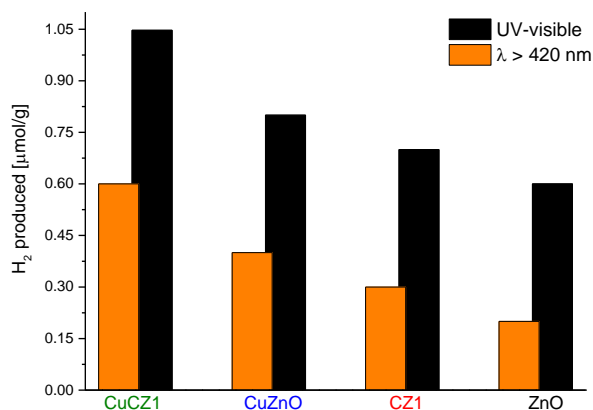

Figure 4. H_2 production over different samples after 2h of irradiation: black bars for UV-visible irradiation, orange bars for band pass filter at λ ≥ 420 nm (solely visible light).

The best performance has been reached for the mixed heterostructure CeO_2-ZnO with CuO_2 loaded at the surface (CuCZ1) upon UV light, with a H_2 production evaluated around 1 μmol/g. In general, the productions were reduced of almost 30% passing from UV-vis to solely visible frequencies. Although in very low amount if compared to the other samples, it could arouse perplexity that also bare ZnO shows some ability in the production of H_2 upon visible light, considering its band gap value: this unexplained photoactivity is due to the presence of energetic levels in ZnO band gap induced by intrinsic defects, as recently investigated in our and others research group.[52] Finally, it can be affirmed that the impregnation of 0.5% in weight of Cu_2O at the photocatalyst surfaces lead to a substantial improvement of the H_2 production through the water photo-splitting process.

3.5 Photodegradation of Tolyltriazol

On the other hand, also the oxidation ability of the prepared materials has been proved, in order to demonstrate the versatility of the engineered photocatalysts. The efficiency of the developed heterojunctions was tested toward the abatement of tolytriazol (TT). Preliminarily, in order to ensure that the reduced TT concentration during the photocatalytic test was due to the activity upon irradiation of the materials, the adsorption in the dark was performed for all samples toward the analyte. In addition, also the photolysis of the molecule in the aqueous environment was examine: in both cases the results were negligible, confirming that the observed degradation aroused from the materials photoactivity.

The degradation profiles obtained for the investigated molecule in the presence of the developed photocatalysts are plotted in Fig. 5; the degradation achieved in the presence of the benchmark TiO_2 P25 is reported as well for comparison purpose. In all cases, the degradation process approximates a pseudo first order kinetic. P25 exhibits the lowest activity (we calculated a kinetic constant of 0.07 min^{-1}) and, considering

the ZnO based materials, the single heterojunction with cerium (CZ1) leads to an increase in the photocatalytic performance (k passes from 0.178 min^{-1} for pristine ZnO to 0.282 min^{-1} for CZ1).

The changes brought to the ZnO matrix by the introduction of Cu_2O slightly increase the performance of the materials. Copper single (Cu_2O-ZnO) and double (Cu_2O-CZ1) heterojunction prompted a faster degradation (the kinetic constant were 0.278 and 0.379 min^{-1} for CuZnO and CuCZ1, respectively), confirming the improved photodegradation ability provided by the Cu oxide loaded on the surface.
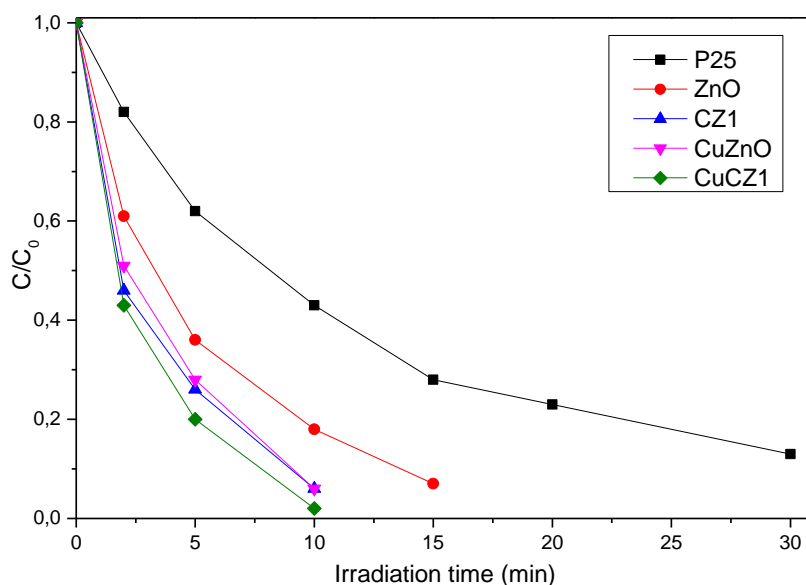

Figure 5. Degradation of tolyltriazol in the presence of the developed photocatalysts.

4. Discussion

The 0.5% in weight Cu_2O surface decoration lead to an appreciable enhance of the already known and extensively studied photocatalysts ZnO and CeO_2-ZnO. The photocatalytic ability improvements were recorded both concerning the reductive and oxidation abilities of the photoinduced charge carriers. In detail, the photo-excited electrons have shown and increased redox capability when Cu_2O phase was loaded, as suggested by the greater H_2 production during the water photosplitting process. On the other hand, also the oxidation power of the photo-formed holes affirmed better performance respect to the non-impregnated systems. Then the proposed surface modification has induced crucial optical and electronic alterations for the ultimate use of the materials as promising photocatalysts.

From a structural point of view, the XRD analysis affirmed that the materials still maintained the wurtzite and cubic lattices fingerprints given by ZnO and CeO_2 phases, respectively; just a very tiny reflection attributable to the cubic Cu_2O phase was registered. The impregnation of Cu_2O greatly affected the optical properties, as testified by the UV-vis analysis. In particular, in addition to the typical band gap absorption of ZnO in the UV region of the electromagnetic spectrum and of the absorption shoulder in the visible region due to the presence of CeO_2 for the mixed systems, a complex profile emerged for the impregnated samples almost from 460 nm to 600 nm. It is clear that the presence of Cu_2O increases the photon absorption in the visible region as expected by the band gap of the material (II in Fig.2). Moreover, other two further phenomena were detected as the charge transfer between the oxide matrix and the impregnated copper(I) (I in Fig. 2, IFCT process), indicating an intimate contact among the different phases, and the presence of a very low amount of metallic copper, identified thanks its typical surface plasmonic effect, resonating around 570 nm (III in Fig. 2).

EPR spectroscopy was instrumental in the detection of Cu^{2+} species coming from an incomplete reduction of all the copper ions provided during the Benedict reduction process. This phenomenon that, in principle, can be considered an imperfection of the synthesis procedure, helped us to further shed the light on the material features under working conditions during the photocatalytic reactions, as discussed in the following.

As first, the intensity of Cu^{2+} detected in both impregnated samples CuZnO and CuCZ1 is almost the same (integration available in S3), meaning that the proposed synthetic route is reproducible. Secondly, it was observed that upon visible irradiation the Cu^{2+} signal intensity is reduced, indicating that the Cu_2O material was resistant to light irradiation without encountering photo-corrosion and that a portion of the deposited Cu^{2+} ions was reduced to Cu^+ or Cu^0. These reasonable deductions lead us to believe that a strong cooperation is established between the impregnated Cu_2O phase and the oxide matrix. Indeed, the decrease of the Cu^{2+} EPR signal can only be explained involving an electronic transfer from the oxide matrix to the Cu^{2+}, that at this point would be reduced; this also would justify the optical absorption at 460 nm (I in Fig. 2). The possible reduction of Cu^{2+} ions on the photocatalyst surfaces is also in line with the redox potentials involved: actually the reductive potential of Cu^{2+} into Cu^+ is 0.16 V (in the NHE), then around 0.2 V below the ZnO conduction band edge. In this way an electron excited in the ZnO conduction band can migrate at lower energy, reducing Cu^{2+} in Cu^+ (IFCT process). In the case of Cu^{2+} reduced into Cu^0, two electrons and a higher potential (0.34 V in the NHE) are needed, limiting the likelihood of the process; nevertheless, although in lower amount, it is reasonable to admit that also this phenomenon could occur, as highlighted by the weak SPR effect trace in the UV-vis spectrum (III in Fig. 2).

The above mentioned and experimentally verified simultaneous charge carrier transfer gives rise to the complex working mechanism of the impregnated CuZnO and CuCZ1 samples. The multistep charge carriers migration at the phases interfaces upon irradiation allows the enhance of the photocatalytic capability of the bare ZnO and of the mixed system CeO_2-ZnO (CZ1) both regarding reductive and oxidative reactions, affirming the polyfunctionality of the synthesized materials in the photocatalytic applications. In order to effectively give a prove of this crucial capacity, two different photocatalytic tests have been arranged. For what concern the evaluation of the redox reductive ability, the amount of H_2 production from the water photosplitting process upon both UV-vis and purely visible irradiation was verified. It emerged that the impregnated samples shown highest activity and the best performance were recorded for CuCZ1. Arguing more in detail these outcomes, we can tentatively discuss the higher H_2 generation for CuCZ1 is due to several concurrent phenomena:

- Firstly, as established in our previous investigations,[31, 40] the interface CeO_2-ZnO allows a larger amount of photoinduced charge carriers stabilized in the solid, lengthening their lifetime. This phenomenon is guaranteed by an electron transfer from ZnO conduction band to the empty, localized *4f* levels of Ce^{4+}, which is reduced to Ce^{3+}. Moreover, the presence of the 4f levels also would extend the photons absorption of the heterojunction into the visible range, as also evidenced by the sample pale yellow color.

- The impregnation of 0.5% of Cu_2O further broadens the visible light harvesting, having a band gap width of 2.4 eV and corresponding to an adsorption edge at 520 nm. Still, the copper (I) oxide is characterized by a more negative flat band potential for the CB respect to bare ZnO,[60] which makes it more suitable for the H_2 generation during the water photosplitting reaction. For this reason, each sample loaded with Cu_2O shows a higher H_2 production compared to the corresponding non-impregnated ones.

- Finally, the non-complete reduction of all Cu^{2+} ions during the Benedict reaction adds additional chemical elements that might be involved in the improvement of the H_2 production. Indeed, by means of EPR technique it has been possible to record the drop of the paramagnetic signal related

to Cu^{2+} species during (visible) irradiation. As extensively discussed, this is an indirect evidence of the photochemical reduction of Cu^{2+} species, coming as "waste" by the synthetic route. Cu^{2+} can be reduced both into Cu^+ and Cu^0 upon illumination: presumably, the formation of a small amount of metallic copper is a key step to explain the enhance of the H_2 amount generated. Actually, metallic copper has been recently indicated as one of the most efficient co-catalysts not based on noble metals such as Pd, Pt and Os.[50, 61-66] This fact is of paramount importance into a widespread consciousness concerning the development of new technologies ever more efficient and based on earth-abundant elements.

Definitely, the reductive ability of the photocatalysts ZnO and CZ1 has been enhanced by the impregnation of Cu_2O onto the surface due to the light induced physical chemistry phenomena listed above, arising from an intimate contact among the different interfaces. At the same time, also the oxidation capability has been improved by the surface impregnation, as testified by the photodegradation of tolytriazol molecule, displaying the synthesized photocatalyst suppleness in the overall photocatalytic process. Indeed, also during the oxidative photocatalytic reaction the 0.5% in weight of Cu_2O loaded at the surface brought to a faster photodegradation of the pollutant molecule. This experimental evidence could again be explained considering the complex band structure at the interfaces of the triphasic material, allowing a better separation of the photo-induced charge carriers in the overall irradiation process. In this regard, an attemping sketch of the possible working mechanism of the triphasic oxide upon visible irradiation in the reductive and oxidative photocatalytic applications has been reported in Fig. 6.
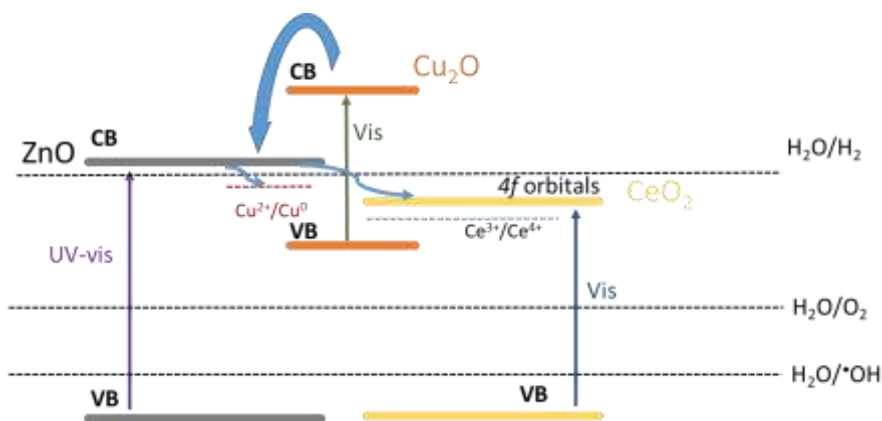

Figure 6. Proposed working mechanism upon irradiation of the triphasic solid Cu_2O-CeO_2-ZnO.

5. Conclusions

In this work both the reductive and oxidative photocatalytic capabilities of the complex triphasic solid Cu_2O-CeO_2-ZnO has been tested and compared with the bare materials. In parallel, the structural, the optical and the electronic features of the prepared samples have been investigated, leading to a detailed picture of the photochemistry characterizing the materials. The outcomes clearly suggest an intimate cooperation at the different interfaces present in the composite heterojunction. In details, although the Cu_2O surface decoration doesn't affect the crystal structure of the impregnated materials, the outcomes provided by EPR and DR-UV-vis spectroscopies clearly establishes that a photochemical transformation occurs in the solid during the irradiation with UV-vis as well as visible light only. It has been observed that during the Benedict reaction involved for Cu_2O precipitation, the deposition on the oxide surface of additional copper species occurs, namely Cu^{2+} and Cu(0). These species are also subjected to the entire electron transfer taking place at the solid interfaces. Accordingly, EPR spectroscopy has highlighted the photo-stability of Cu_2O surface; moreover, it indicates the electronic transition from the oxide matrix to Cu^{2+}, reduced to metallic copper, as

suggested by the reduction of the Cu^{2+} signal upon illumination. Consequently, the photoinduced formation of Cu(0) could act as a co-catalyst in the H_2 evolution process from the water photosplitting, explaining the improved reductive abilities. Finally, also a better photodegradation performance has been recorded for Cu_2O-CeO_2-ZnO in the abatement of the tolytriazol pollutant: once again, the intimate contact between the complex interfaces allows a better spatial separation of the photoinduced charge carriers, enhancing the oxidative process carried on by holes.

Concluding, notwithstanding some fundamental aspects still needs targeted insights in order to further increase the photocatalytic abilities of the developed material, as the optimal loading percentage of Cu_2O, the exploitation of other deposition methods and the actual role of metallic copper, the Cu_2O-CeO_2-ZnO triphasic heterosystem has revealed a unique versatility in the overall photocatalytic process.

Acknowledgments

References

1. A. Kubacka, M. Fernandez-Garcia and G. Colon, *Chem. Rev.*, 2012, **112**, 1555-1614.
2. T. Hisatomi, J. Kubota and K. Domen, *Chem. Soc. Rev.*, 2014, **43**, 7520-7535.
3. A. Hernandez-Ramirez and I. Medina-Ramirez, *Photocatalytic Semiconductors*, Switzerland, 2014.
4. A. Fujishima and K. Honda, *Nat. Biotechnol.*, 1972, **238**, 37-38.
5. N. N. Vu, S. Kaliaguine and T. O. Do, *Adv. Funct. Mater.*, 2019, **29**, 1901825.
6. Q. Xu, L. Zhang, J. Yu, S. Wageh, A. A. Al-Ghamdi and M. Jaroniec, *Mater. Today*, 2018, **21**, 1042-1063.
7. N. Subha, M. Mahalakshmi, M. Myilsamy, B. Neppolian and V. Murugesan, *Appl. Catal., A*, 2018, **553**, 43-51.
8. M. R. Hoffman, S. T. Martin, W. Choi and D. W. Bahnemann, *Chem. Rev.*, 1995, **95**, 69-96.
9. D. Ravelli, D. Dondi, M. Fagnoni and A. Albini, *Chem. Soc. Rev.*, 2009, **38**, 1999-2011.
10. A. Folli, J.Z. Bloh, M. Strom, T.P Madsen, T. Henriksen and D. E. Macphee, *J. Phys. Chem. Lett.*, 2014, **5**, 830-832.
11. U. Özgür, Y. I. Alivov, C. Liu, A. Teke, M. A. Reshchikov, S. Doğan, V. Avrutin, S. J. Cho and H. Morkoç, *J. Appl. Phys.*, 2005, **98**, 041301-041301103.
12. A. Moezzi, A. M. McDonagh and M. B. Cortie, *Chem. Eng. J.*, 2012, **185-186**, 1-22.
13. C. Klingshirn, J. Fallert, H. Zhou, J. Sartor, C. Thiele, F. Maier-Flaig, D. Schneider and H. Kalt, *Phys. Stat. Sol. B*, 2010, **247**, 1424-1447.
14. A. Mang, K. Reimann and S. Rubenacke, *Solid State Commun.*, 1995, **94**, 251-254.
15. A. Janotti and C. G. Van de Walle, *Phys. Rev. B*, 2007, **75**, 1212011-1212014.
16. S. Rehman, R. Ullah, A.M. Butt and N. D. Gohar, *J. Hazard. Mater.*, 2009, **170**, 560-569.
17. B. Abebe, H. C. A. Murthy and E. Amare, *Environ. Nanotechnol. Monit. Manag.*, 2020, **14**, 100336.
18. B. Al Farsi, F. Al Marzouqi, M Al-Maashani, M.T. Souier, M.T. Myint and M. Z. Al-Abri, *Mater. Sci. Eng., B*, 2021, **264**.
19. R. Mahdavi and S. S. Talesh, *Adv. Power Technol.*, 2017, **28**, 1418-1425.
20. H. Liu, L. Zhong, S. Govindaraju and K. Yun, *J. Phys. Chem. Solids*, 2019, **129**, 46-53.
21. N.A. Putri, V. Fauzia, S. Iwan, L. Roza, A. Ali Umar and S. Budi, *Appl. Surf. Sci.*, 2018, **439**, 285-297.
22. C. Han, L. Duan, X. Zhao, Z. Hu, Y. Niu and W. Geng, *J. Alloys Compd.*, 2019, **770**, 854-863.
23. V. Vaiano, G. Iervolino and L. Rizzo, 2018, **238**, 471-479.

24. N.P.F. Goncalves, M.C. Paganini, P. Armillotta, E. Cerrato and P. Calza, *J. Environ. Chem. Eng.*, 2019, **7**, 106475.
25. A.B. Patil, K.R. Patil and S. K. Pardeshi, *J. Hazard Mater*, 2010, **183**, 315-323.
26. O. Haibo, H.J. Feng, L. Cuiyan, C. Liyun and F. Jie, *Mater. Lett.*, 2013, **111**, 217-220.
27. C. Gionco, D. Fabbri, P. Calza and M. C. Paganini, *J. Nanomater.*, 2016, 1-7.
28. E. Cerrato and M. C. Paganini, *Mater. Adv.*, 2020, **1**, 2357.
29. Y. Li, M. Zhou, B. Cheng and Y. Shao, *J. Mater. Sci. Technol.*, 2020, **56**, 1-17.
30. P. Calza, C. Gionco, M. Giletta, M. Kalaboka, V. A. Sakkas, T. Albanis and M. C. Paganini, *J. Hazard. Mater.*, 2016, **323**, 471-477.
31. E. Cerrato, C. Gionco, M. C. Paganini, E. Giamello, E. Albanese and G. Pacchioni, *ACS Appl. Energy Mat.*, 2018, **1**, 4247-4260.
32. S. Banerjee, *Europhys. Lett.*, D. Chakravorty, **52**, 468-473.
33. N. E. Markina, M. V. Pozharov and A. V. Markin, *J. Chem. Educ.*, 2016, **93**, 704-707.
34. F. Vines, O. Lamiel-Garcia, K. Chul Ko, J.Y. Lee and F. Illas, *J. Comput. Chem.*, 2017, **38**, 781-789.
35. R. Li, L. Yu, X. Yan and Q. Tang, *RSC Adv.*, 2015, **5**, 11917.
36. X-S Wang, Y-D Zhang, Q-C Wang, B. DOng, Y-J Wang and W. Feng, *Sci Eng Compos Mater*, 2019, 104-113.
37. K. P. Musselman, A. Marin, A. Wisnet, C. Scheu, J. L. MacManus-Discroll and L. Schmidt-Mende, *Adv. Funct. Mater.*, 2011, 573-582.
38. J. Cui and U. J. Gibson, *J. Phys. Chem. C*, 2010, **114**, 6408-6412.
39. G. Martra, E. Gianotti and S. Coluccia, in *Metal Oxide Catalysis*, eds. S. D. Jackson and J. S. J. Hargreaves, WILEY-VCH Verlag GmbH & Co. KGaA, Weinheim, 2009, pp. 51-94.
40. E. Cerrato, C. Gionco, M. C. Paganini and E. Giamello, *J. Phys. Condens. Mattter.*, 2017, **29**, 1-7.
41. E. Cerrato, C. Gionco, I. Berruti, F. Sordello, P. Calza and M. C. Paganini, *J. Solid State Chem.*, 2018, **264**, 42-47.
42. T. D. Golden, M. G. Shumsky, Y. Zhou, R. A. VanderWerd, R. A. Van Leeuwen and J. A. Sweitzer, *Chem. Mater.*, 1996, **8**, 2499-2504.
43. A. Ashrafi and C. Jagadish, *J. Appl. Phys.*, 2007, **102**, 071101.
44. V. Srikant and D. R. Clarke, *J. Appl. Phys.*, 1998, **83**, 5447-5451.
45. A. Janotti and C. G. V. d. Walle, *Phys. Rev. B*, 2007, **76**, 165202-16520222.
46. F. Oba, M. Choi, A. Togo and I. Tanaka, *Sci. Technol. Adv. Mater.*, 2016, **12**, 034302.
47. Juarez L. F. Da Silva, M. Verónica Ganduglia-Pirovano and J. Sauer, *Phys. Rev. B*, 2007, **75**, 045121.
48. I. Tamiolakis, I. T. Papadas, K. C. Spyridopoulos and G. S. Armatas, *RSC Advances*, 2016, **6**, 54848-54855.
49. H. Tada, Q. Jin, H. Nishijima, H. Yamamoto, M. Fujishima, S. Okuoka, T. Hattori, Y. Sumida and H. Kobayashi, *Angew Chem Int Ed Engl*, 2011, **50**, 3501-3505.
50. V. Polliotto, S. Livraghi, A. Krukowska, M. V. Dozzi, A. Zaleska-Medynska, E. Selli and E. Giamello, *ACS Appl Mater Interfaces*, 2018, **10**, 27745-27756.
51. M. A. Sliem, T. Hikov, Z. A. Li, M. Spasova, M. Farle, D. A. Schmidt, M. Havenith-Newen and R. A. Fischer, *Phys Chem Chem Phys*, 2010, **12**, 9858-9866.
52. E. Cerrato, M. C. Paganini and E. Giamello, *J. Photochem. Photobiol., A*, 2020, **397**, 112531.
53. D. M. Hofmann, A. Hofstaetter, F. Leiter, H. Zhou, F. Henecker, B. K. Meyer, S. B. Orlinskii, J. Schmidt and P. G. Baranov, *Phys. Rev. Lett.*, 2002, **88**, 0455041-0455044.
54. P. H. Kasai, *Phys. Rev.*, 1963, **130**, 989-995.
55. S. M. Evans, N. C. Giles, L. E. Halliburton and L. A. Kappers, *Journal of Applied Physics*, 2008, **103**, 043710.
56. N. Kondal and S. K. Tiwari, *Mater. Res. Bull.*, 2017, **88**, 156-165.
57. R. Buchheit, F. Acosta-Humanez and O. Almanza, *Rev. Cub. Fis.* , 2016, **33**, 4-12.
58. T. Sreethawong and S. Yoshikawa, *Int. J. Hydrogen Energy*, 2006, **31**, 786-796.
59. F. Parveen, B. Sannakki, M. V. Mandke and H. M. Pathan, *Sol. Energy Mater. Sol. Cells*, 2016, **144**, 371-382.
60. Y. Xu and M. A. Schoonen, *Am. Mineral.*, 2000, **85**, 543-556.

61. M. Chaudhary, S.-m. Chang, R.-a. Doong and H.-m. Tsai, *J. Phys. Chem. C*, 2016, **120**, 21381-21389.
62. Z. Xi, C. Li, L. Zhang, M. Xing and J. Zhang, *Int. J. Hydrogen Energy*, 2014, **39**, 6345-6353.
63. T. Montini, V. Gombac, L. Sordelli, J. J. Delgado, X. Chen, G. Adami and P. Fornasiero, *ChemCatChem*, 2011, **3**, 574-577.
64. X.-J. Lv, S.-X. Zhou, C. Zhang, H.-X. Chang, Y. Chen and W.-F. Fu, *J. Mater. Chem.*, 2012, **22**, 18542.
65. H. Tian, S.-Z. Kang, X. Li, L. Qin, M. Ji and J. Mu, *Sol. Energy Mater. Sol. Cells*, 2015, **134**, 309-317.
66. D. Ni, H. Shen, H. Li, Y. Ma and T. Zhai, *Appl. Surf. Sci.*, 2017, **409**, 241-249.